Title

Palladized cells as suspension catalyst and electrochemical catalyst for reductively degrading aromatics contaminants: Roles of Pd size and distribution

Authors

Hou, Ya-Nan

Zhang, Bo

Yun, Hui

et al.

Publication Date

2017-11-01

DOI

10.1016/j.watres.2017.08.055

Peer reviewed

Palladized cells as suspension catalyst and electrochemical catalyst for reductively degrading aromatics contaminants: Roles of Pd size and distribution

Author links open overlay panelYa-NanHou[a]BoZhang[b]HuiYun[b]Zhen-NiYang[b]Jing-LongHan[b]JizhongZhou[ac]Ai-JieWang[ab]Hao-YiCheng[b]
Show more

https://doi.org/10.1016/j.watres.2017.08.055Get rights and content

Highlights

- The size and distribution of Pd-cell NPs are affected by the ratio of CDW to Pd.
- The quantitative characterization strategy of Pd associate with cell is proposed.
- Pd-cell can be used as valid catalyst for the catalytic reduction of NB and 4-CP.
- Catalytic activity of suspended Pd-cell catalyst is ruled by exposed area of Pd NP.
- The conductivity of electrocatalyst Pd-cell determines its catalytic effectiveness.

Abstract

The palladized cell (Pd-cell) could be used as an efficient catalyst in catalyzing the degradations of a wide variety of environmental contaminants. Nevertheless, when the Pd NPs associate with the bacteria, the catalytic activity likely significantly affected by the biomass. Quantitative indicators that characterize of Pd-cell are necessary and little attention has been paid to investigate how the catalytic efficiency of Pd-cell is affected by the size and distribution of Pd NPs. To fill this gap, we explored the roles of the above-mentioned key factors on the performance of Pd-cell in catalyzing the degradations of two aromatic contaminants (nitrobenzene and *p*-chlorophenol) in two commonly used scenarios: (1) using Pd-cell as suspended catalyst in solution and (2) using Pd-cell as electrocatalyst directly coated on electrode. In scenario (1), the

relationship of exposing area to Pd particle size and distribution factors was established. Based on theoretical estimation and catalytic performance analysis, the results indicated that adjusting the exposing area to a large value ($9.3 \pm 0.1 \times 10^5$ nm^2 mg^{-1} Pd) was extremely effective for improving the catalytic activity of Pd-cell used as a suspension catalyst. In scenario (2), our results showed that the best electrocatalytic performances were achieved on the electrode decorated with Pd-cells with the largest NP size (54.3 ± 16.4 nm), which exerted maximum electrochemical active surface area (10.6 m^2 g^{-1}) as well as favorable conductivity. The coverage of deposited Pd NPs (>95%) on the cell surface played a crucial role in boosting the conductivity of biocatalyst, thus determining the possibility of Pd-cell as an efficient electrocatalyst. The findings of this study provide a guidance for the synthesis and application of Pd-cell, which enables the design of Pd-cell to be suitable for different catalysis systems with high catalytic performance.

Graphical abstract

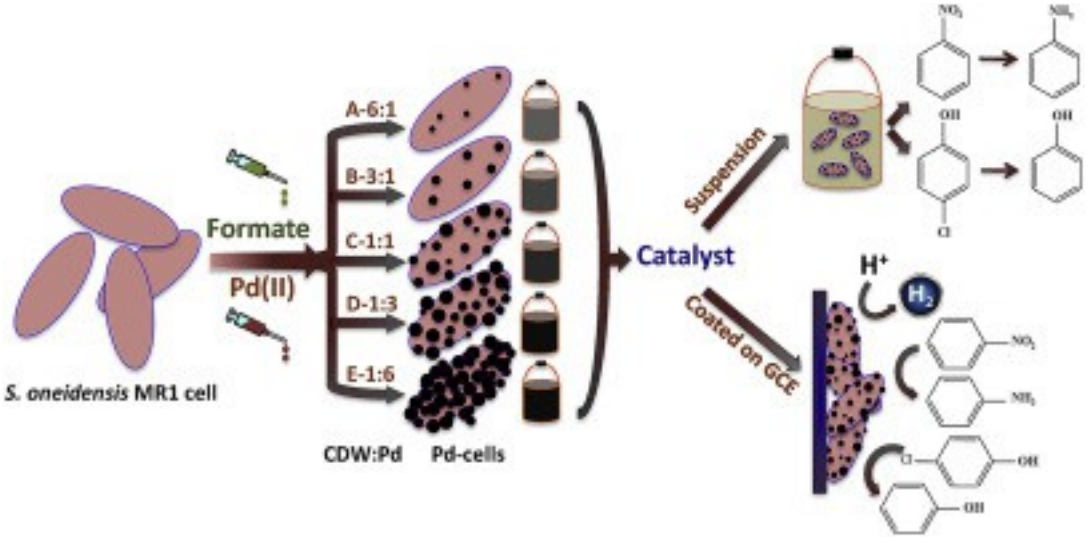

1. Download high-res image (297KB)
2. Download full-size image

- **Previous** article
- **Next** article

Keywords

Palladium
Nanoparticle size
Catalytic activity
Nitrobenzene

p-chlorophenol

1. Introduction

Palladium (Pd)-based catalysis has been considered as a promising water treatment strategy, as Pd has exceptional capability in providing atomic H and can catalyze the reductive transformation of a number of priority contaminants (e.g., chlorinated compounds, oxyanions and aromatics)(Hosseinkhani et al., 2013, And and Reinhard, 1999, Chaplin et al., 2012, Cortese and Heck, 1977, Davie et al., 2006). A variety of chemical and physical procedures could be used for the synthesis of Pd nanoparticles. However, these methods suffer from several issues including the use of toxic solvents, generation of hazardous by-products, and high energy consumption(Nemamcha et al., 2006). Accordingly, the biological inspired methods have been developed as an efficient and eco-friendly approach. The topic regarding to biogenic Pd (bioPd) NPs has received extensive interests recently(Narayanan and Sakthivel, 2010, Wu et al., 2011, Hennebel et al., 2012, Pat-Espadas et al., 2014, Tuo et al., 2015, Hou et al., 2016, Windt et al., 2005).

Pd NPs synthesized by bacteria cells is particularly attractive in the scope of the bio-Pd. Because the incubation of bacteria is simple, fast and cost-effective, this approach holds great potential on the green synthesis of Pd NPs at large scale. A number of bacteria have been demonstrated to produce Pd NPs, such as *Desulfovibrio desulfuricans, Shewanella oneidensis, Geobacter sulfurreducens,* to name a few(Pat-Espadas et al., 2014, Windt et al., 2005, Yong et al., 2002a). The cells not only play the role as the synthesizer through the enzymatic (e.g. hydrogenase and cytochromes) reactions to catalyze the reduction of Pd(II) to Pd(0), but also as the stabilizer to bound the Pd NPs and avoid their aggregation(Pat-Espadas et al., 2014, Mikheenko et al., 2008). The palladized cell (Pd-cell) is capable of being as an efficient catalyst without further treatment. For environmental purpose, the catalysis of Pd-cell has been realized in the reductive dehalogenation of chlorinated compounds, nitroaromatic compounds and chromate reduction, etc(Hosseinkhani et al., 2013, Tuo et al., 2013, Tuo et al., 2015, Martins et al., 2017).

The particle size, a vital importance character of catalyst, would definitely affect surface-to-volume ratio and electronic structure, which determines the catalytic properties of a nanocrystal-based material(Zhou et al., 2006, Li et al., 2002, Shao et al., 2011, Sun and Zeng, 2002, Mistry et al., 2016). Macaskie et al. also suggested that the catalytic activity of the bioPd NPs was related to the NPs size, e.g. the estimated surface area of bioPd formed by *D. desulfuricans* was 3.5-fold greater than the *E. coli* fabricated bio-Pd

NPs, which was in agreement with the difference in catalytic activities toward Cr(VI) reduction and polychlorinated biphenyls (PCBs) dehalogenation(Macaskie et al., 2012). Nevertheless, when the Pd NPs associate with the bacteria in the Pd-cell, the impact factors on the catalytic activity may differ from those in the chemically synthesized Pd NPs and likely significantly affected by the biomass. Normally, catalytic activity of Pd NPs takes place on the particles surface. Boon et al. investigated the catalytic dechlorination activity of suspended and immobilized bioPd NPs, which demonstrated the entrapment of Pd NPs in a polymeric matrix could be a reason for decreasing the potential of catalysts in removing contaminants(Hosseinkhani et al., 2015). The resulting catalytic activity of the Pd-cell is a function of both the initial crystal nucleation and the subsequent bioreduction to Pd(0)(Yong et al., 2002b). The Pd-cell catalysts showed variable activity for a given reaction probably attributable to strain-specific differences in cell surface(Deplanche et al., 2010, Deplanche et al., 2014). It had also been found that the relatively large and densely Pd(0) crystals covered on biomass exhibited high catalytic activity towards the degradation of hydrophobic molecules, such as polychlorinated biphenyls(De Windt et al., 2006). That means when cell bound Pd NPs are used for catalytic purpose, besides size effects, other factors such as NPs location, exposed area and the degree of NPs coverage on cell surface may also affect the catalytic activity. To date, the knowledge of these properties is limited and the relevant quantitative characterization is not clear yet.

In addition to being used as suspension catalyst, Pd-cell can also be used as an electrocatalyst, immobilized on the electrode surface, e.g. the cathode can be employed to produce H_2 in a sustainable way to provide an economical interesting reactant for bio-Pd catalyzed dehalogenation reactions. It is of great interest to examine the impact of decorated electrode on the performance of contaminants removal such as diatrizoate degradation and chlorinate hydrocarbons reduction(Hosseinkhani et al., 2013, De Gusseme et al., 2011, Hennebel et al., 2011). Studies have demonstrated that bioPd decorated electrode enhanced the efficiency of contaminants removal(Hosseinkhani et al., 2013, De Gusseme et al., 2011, Hennebel et al., 2011). However, this kind of Pd-cell have rarely been used as electrocatalyst directly because of the poor conductive nature of microbial cells(Liu et al., 2016, Xiong et al., 2015). The biomass associated with the Pd NPs maintained as a physical nonconductive supporter. High-temperature carbonization and pyrolysis are the common approaches to increase the conductivity of microbial matrix(Yates et al., 2014). However, these post processes require additional energy and the aggregation of those nanoparticles at high temperature would limit their catalytic performance(Sun et al., 2012). To the best of our knowledge, no

comprehensive study has been conducted to investigate the effects of the bio-Pd size as well as the distribution properties on the electrocatalytic reduction performance of bioPd.

The present study aims to put forward the quantitative indicators to characterized the cell associated Pd NPs and investigate the effects of these indicators on the catalytic performance towards catalyzing aromatic contaminants (nitrobenzene and *p*-chlorophenol) reduction in suspension and electrochemical catalysis systems. Pd-cells were produced using *Shewanella Oneidensis* MR-1 at different cell dry weight to Pd(II) weight (CDW:Pd) ratios with formate as the reductant. Four quantitative indicators including size, extracellular distribution degree, exposing active area and coverage percentage on the cell surface were proposed to characterize the cell associated Pd NPs. The correlations between these indicators and the catalytic performance of Pd-cell were explored in above-mentioned two types of catalysis systems and the principle for Pd-cell being used as suspension catalyst or electrochemical catalyst was proposed. This work provides new perspective on designing bio-Pd, enabling this eco-friendly catalyst to be highly efficient when applying into the two commonly used treatment systems.

2. Materials and methods

2.1. Bacterial strains and culture conditions

Shewanella oneidensis MR-1 was aerobically cultured in Luria-Bertani (LB) medium(Sambrook and Russell, 2001) at 30 °C on a rotary shaker with the shaking speed of 120 rpm overnight. Then the *S. oneidensis* cells were harvested by centrifugation (6000 *g*, 10 min) and washed three times with sterile phosphate buffer solution (PBS) that was consisted of $NaH_2PO_4 \cdot 2H_2O$ (2.77 g/L), $Na_2HPO_4 \cdot 12H_2O$ (11.55 g/L), KCl (0.13 g/L) and NH_4Cl (0.31 g/L).

2.2. Preparation of Pd-cells with different CDW:Pd ratios

The washed cells were resuspended in anaerobic PBS to a final CDW concentration of 919.5, 450.5, 150.3, 51.9 and 25.8 mg L^{-1}. To prepare Pd-cell with CDW:Pd ratios of 6:1 (group A), 3:1 (group B), 1:1 (group C), 1:3 (group D) and 1:6 (group E), formate (1 M) and Pd(II) (1 g L^{-1}) stock solutions were added as electron donor and acceptor to a final concentration of 25 mM and 150 mg L^{-1}, respectively. The above-mentioned bio-reduction serum bottles were anaerobically incubated at 30 °C. All assays were set up in triplicate.

2.3. Characterization of Pd-cells

The samples for field emission scanning electron microscope(FESEM) were fixed overnight in phosphate buffer solution (PBS, 10 mM, pH 7.0) with 2.5% glutaraldehyde, dehydrated in a graded series of ethanol (50, 70, 80, 90, and 3 × 100% with 15 min for each level), displaced by 50% isoamyl acetatein ethanol and 100% isoamyl acetate sequentially for 15min each, and dried in a desiccator for 12 h. The prepared samples were then observed using a FESEM (SU8000, Hitachi Ltd, Japan) operated at 3 kV. Elemental analysis was performed using the electron dispersive spectroscopy (EDS) detector, which was equipped on the FESEM.
Samples for transmission electron microscopy (TEM) ultramicrotomy were fixed in 2.5% glutaraldehyde overnight and stained with 1% osmium tetroxide for 1 h, dehydrated in graded series of ethanol (same as in FESEM samples preparation). The samples were then embedded in Eponate resin, sliced into pieces with a thickness of 70 nm by an ultramicrotome (Ultracut UCT, Leica Microsystems IR GmbH, Germany) and observed with a TEM (JEM-1400, JEOL).
X-ray diffraction (XRD) measurements were performed on a PANalytical PW 3050 Philips X'pert Pro with Cu Kα radiation (λ = 1.541 Å). The aqueous concentrations of Pd were measured with ICP-OES (Leeman labs Prodigy).

2.4. Estimation of exposed area of Pd-cell NPs

The estimation of the exposed area (S_{exp}) was made based on the assumption that each nanoparticle was spherical and only the extracellularly distributed Pd NPs were considered to be exposed. Five randomly selected TEM images were analyzed using the software Image-Pro Plus 6.0 and the average particle diameter obtained was used to calculate the surface area (S_u) and volume of individual NPs. The number of NPs (N) per milligram of Pd was estimated based on the volume and density of individual NPs. The extracellular distribution degree of Pd NPs (f_{ext}) was calculated according to the ratio of Pd NPS located outside of the cells which was estimated based on the TEM images and statistical analysis using the software Image-Pro Plus 6.0 (examples of this estimation can be found in the Supporting Information, SI). The calculation for exposed area can be simplified as:

$$(1) S_{exp} = S_u \times N \times f_{ext}/2$$

where S_u is the surface area of individual NPs, N is the number of NPs in per milligram of Pd, f_{ext} is the extracellular distribution degree of NPs.

2.5. Preparation of Pd-cell decorated electrodes

The synthesized Pd-cell with different CDW:Pd from 6:1 to 1:6 (groups A, B, C, D and E) were separated by centrifugation and washed with PBS three times before they were coated onto the surface of pre-polished glassy carbon electrode(GCE, 0.126 mm^2). The amount of Pd that was immobilized on the bacterial surface in each group was calculated based on the aqueous concentration of Pd before and after the biological reduction reaction. With this piece of information, we were able to control the loading of Pd to be 100 μg cm^{-2}throughout this study. The Pd-cell decorated electrodes were dried at room temperature for 12 h before they were used for electrochemical measurements.

2.6. Pd-cell used as suspension catalyst in catalytic reduction of NB and 4-CP

The prepared Pd-cells were mixed with aqueous NB (25 mL, 100 mg L^{-1}) and freshly prepared $NaBH_4$ solution (25 mL, 1 g L^{-1}) in a serum bottle. According to the Pd mass content in the Pd-cells obtained under different CDW:Pd ratios conditions, the content of Pd in different suspension catalysissystems were adjusted to be identical (2.0 mg L^{-1} Pd in the reaction system). Samples were taken at regular intervals and filtered through a 0.22 μm filter in prior to analysis.

The concentrations of nitrobenzene were measured using a high performance liquid chromatography system (LC-20AT, Shimadzu, Japan) equipped with a Waters Symmetry C18 column (5 μm 4.6 × 250 mm) for separation at 35 °C and a diode array detector (SPD-M20A, Japan) for measurement at 254 nm. The reduction of 4-CP was also tested following similar procedures with initial 4-CP concentration of 135 mg L^{-1}.

2.7. Electrochemical measurements

The electrochemical measurements were taken in a gas-tightsingle-chamber, three-electrode system, using a multi-channel potentiostat (1030C, CH Instruments Inc, U.S.). The system was flushed with high-purity nitrogen gas for 15 min to obtain N_2-saturated solution before the electrochemical tests. The Pd-cell decorated glassy carbon electrodes were used as working electrodes. The platinum mesh (100 mm^2) and Ag/AgCl electrode (in saturated KCl solution, +197 mV vs standard hydrogen electrode) were used as counter and reference electrodes, respectively. In order to calculate the electrochemical active surface area (ECSA), cyclic voltammetry (CV) of each bio-catalyst coated electrode was performed in 50 mM PBS solution with the scan rate of 10 mV s^{-1} in the potential range from −0.55–0.8 V vs Ag/AgCl. The ECSA was calculated according to(Zhao et al., 2011):

(2)$ECSA = Q/(0.405 \times Pd_m)$

where Pd_m is the Pd mass loaded on the surface of working electrode, charges (Q) associated with the peak from reduction of Pd(II) oxide.
The hydrogen evolution reaction (HER) was investigated by cyclic voltammetry (CV) scanning in potential range from 0.1 to −1.0 V with the scan rate of 10 mV s^{-1} in 50 mM oxygen-free PBS. Also, chronoamperometry (CA) was performed at a constant potential of −0.7 V for HER and −0.55 V for NB and 4-CP reduction with a time frame of 5 h. Electrochemical impedance spectroscopy (EIS) measurement was implemented using the same electrode system with the frequency from 10 MHz to 0.01 Hz. All potentials were reported with respect to Ag/AgCl in this study.

2.8. Conductivity calculation

According to the two-probe measurements used for biofilmconductivity testing (Malvankar et al., 2011), a customized screen-printed gold electrode (SPGE, with a geometric working area of 1 cm^2) with a non-conductive gap (100 μm) in the middle of working area, which splits the conductive area into two parts, was used to measure the currents and bias voltages, and a voltage ramp of 0 V–0.05 V was applied across this split electrodes in steps of 0.001 V by electrochemical workstation (CH Instruments, U.S.). The obtained current–voltage curves from this test (I–V) were used to calculate the conductance (i.e. the slope of the I-V curve). The conductivity (σ) of the coating layer was calculated according to Eq. (3): (Malvankar et al., 2011)

$$\sigma = (G\pi/L)/\ln(8g/\pi a) \quad (3)$$

where G is the conductance; L is the length of the electrodes (L≈1 cm); a is the half-spacing between the electrodes (2a≈100 μm) and g is the coating layer thickness measured using SEM (figure not shown).

3. Results and discussion

3.1. Synthesis and characterization of Pd-cell with different CDW:Pd ratios

The schematic diagram of Pd-cell synthesis and application were shown in Fig. 1. To prepare Pd-cells, formate and Pd (II) were added as electron donor and acceptor, respectively, to the suspension of *S. Oneidensis* MR-1. By adjusting the ratio of biomass (CDW) to Pd(II), five groups (A, B, C, D and E for the CDW:Pd ratio at 6:1, 3:1, 1:1, 1:3 and 1:6, respectively) of Pd-cells were obtained. After injection of Na_2PdCl_4, the color of the liquid medium in all serum bottles changed gradually from yellow to black as time elapsed. As indicated by the removal of aqueous Pd(II) (Table 1), the color change was a result of the reduction of Pd(II) to Pd(0)(Hennebel et al., 2012). The above-prepared Pd-cells were subsequently applied as the catalyst either in suspended system or

electrochemical system (immobilized Pd-cell directly on GCE surface) to reductively degrading aromatic compounds. The morphologies of the bacterial based NPs were observed by FESEM as shown in Fig. 2. For samples obtained from the treatments with high CDW:Pd ratios, i.e. relatively low Pd(II) concentration, the formed NPs were scattered on the cell membrane (Fig. 2A, B, F and G) while those obtained under low CDW:Pd ratio conditions represent a thick layer of Pd on the cell surface with the formation of bulk particles as well (circled in red in Fig. 2, E, J and O).

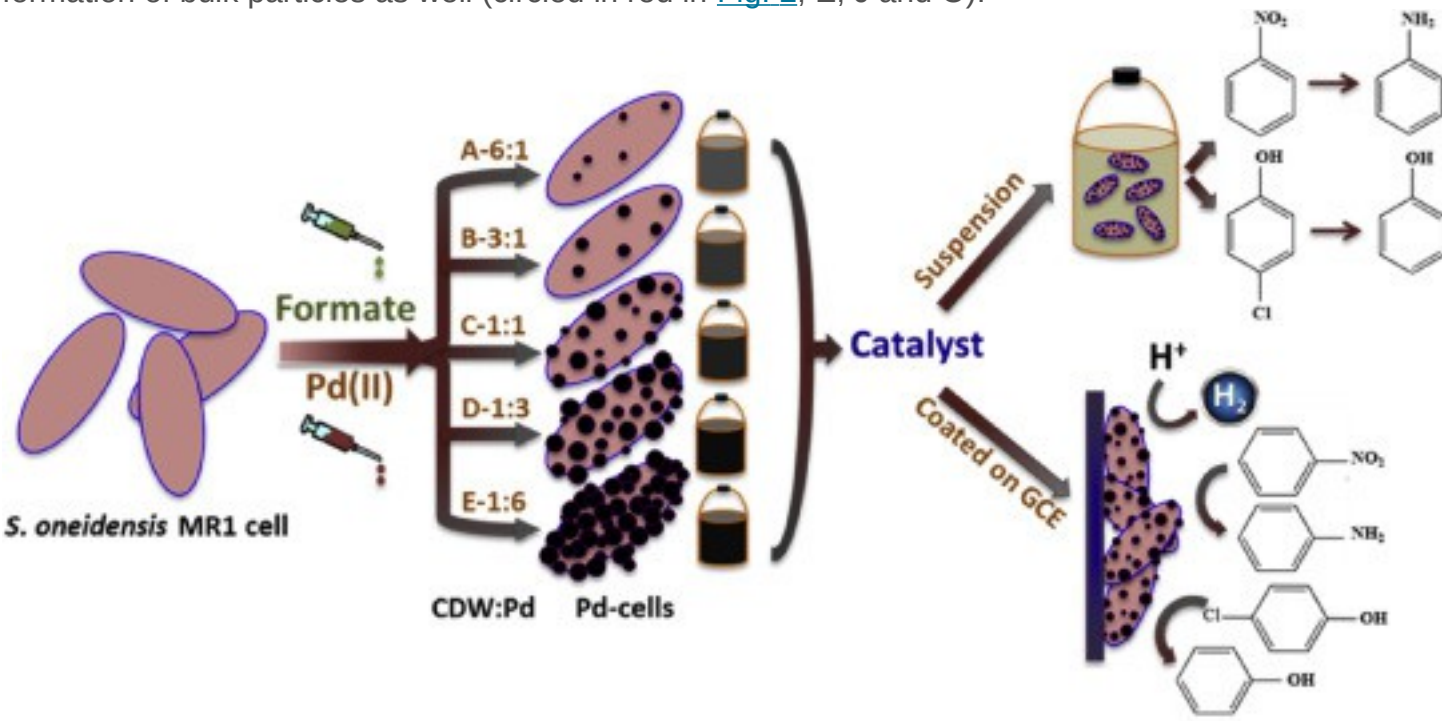

1. Download high-res image (332KB)
2. Download full-size image

Fig. 1. Schematic of fabrication procedure for Pd-cell catalyst with different cell dry weight to Pd (CDW:Pd) ratios apply in two systems: suspension and electrochemical (coated on electrode) used for catalyzing NB and 4-CP reduction.

Table 1. Pd(II) removal and the average size, exposed area of synthesized bioPd in different cell dry weight to Pd ratios.

Catalyst (CDW:Pd)	Group A 6:1	Group B 3:1	Group C 1:1	Group D 1:3	Group E 1:6
CDW (mg L^{-1})	919.5	450.5	150.3	51.9	25.8
Initial Pd II concentration (mg L^{-1})	151.1 ± 2.3	150.9 ± 1.7	149.3 ± 4.5	153.3 ± 3.7	154.6 ± 3.0
Final Pd II concentration	0.9 ± 0.2	0.9 ± 0.3	1.0 ± 0.4	1.7 ± 0.4	2.7 ± 0.7

Catalyst (CDW:Pd)	Group A 6:1	Group B 3:1	Group C 1:1	Group D 1:3	Group E 1:6
(mg L^{-1})					
Removal efficiency (%)	99.3 ± 0.1	99.4 ± 0.5	99.4 ± 0.3	98.9 ± 0.2	98.3 ± 0.4
Average diameter (nm)	7.7 ± 3.9	10.5 ± 4.8	20.6 ± 12.5	25.8 ± 7.8	54.3 ± 16.4
Exposed area of per mg Pd × 10^5(nm^2 mg^{-1})	6.7 ± 0.8	8.2 ± 1.4	10.6 ± 0.3	9.3 ± 0.1	4.5 ± 0.1

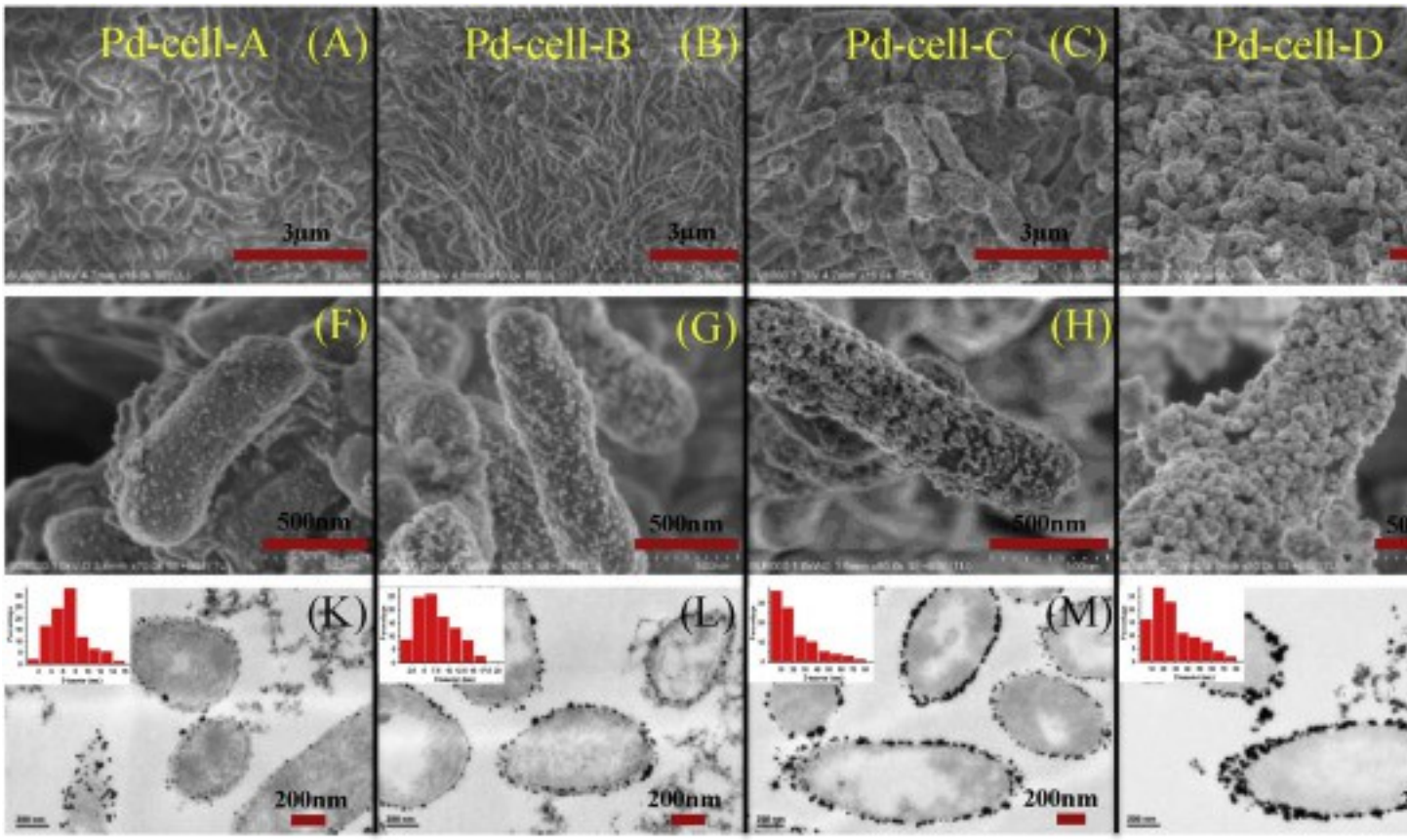

1. Download high-res image (927KB)
2. Download full-size image

Fig. 2. Pd-cells characterization. (A)–(E) SEM images and corresponding (F)–(J) enlarged SEM, (K)–(O) TEM images of the ultrathin slice of series Pd-cells at the ratio of CDW:Pd from 6:1 to 1:6 and their corresponding size distribution histograms, respectively. Red circled in Fig. E, J and O represent aggregate bulk particles. (For interpretation of the references to colour in this figure legend, the reader is referred to the web version of this article.)

EDS analysis confirmed the elemental composition of the synthesized nanoparticles (Fig. 3A). The strong peak at 3 keV indicated that the observed nanoparticles was elemental Pd. Other existing elements revealed by the EDS analysis included carbon and oxygen, which may originate from bacteria cells and cell-excreted extracellular polymeric substances (EPS) responsible for reducing, capping and stabilization of the Pd nanoparticles. The crystalline nature of these synthesized Pd-cell catalysts was also determined by XRD spectroscopy (Fig. 3B). In the diffractogram, all samples showed four distinct reflections at 39.8° (111), 46.5° (200), 68° (220), 82° (311), which indicated that the face centered cubic (fcc) crystalline was the prominent structure for Pd NPs.

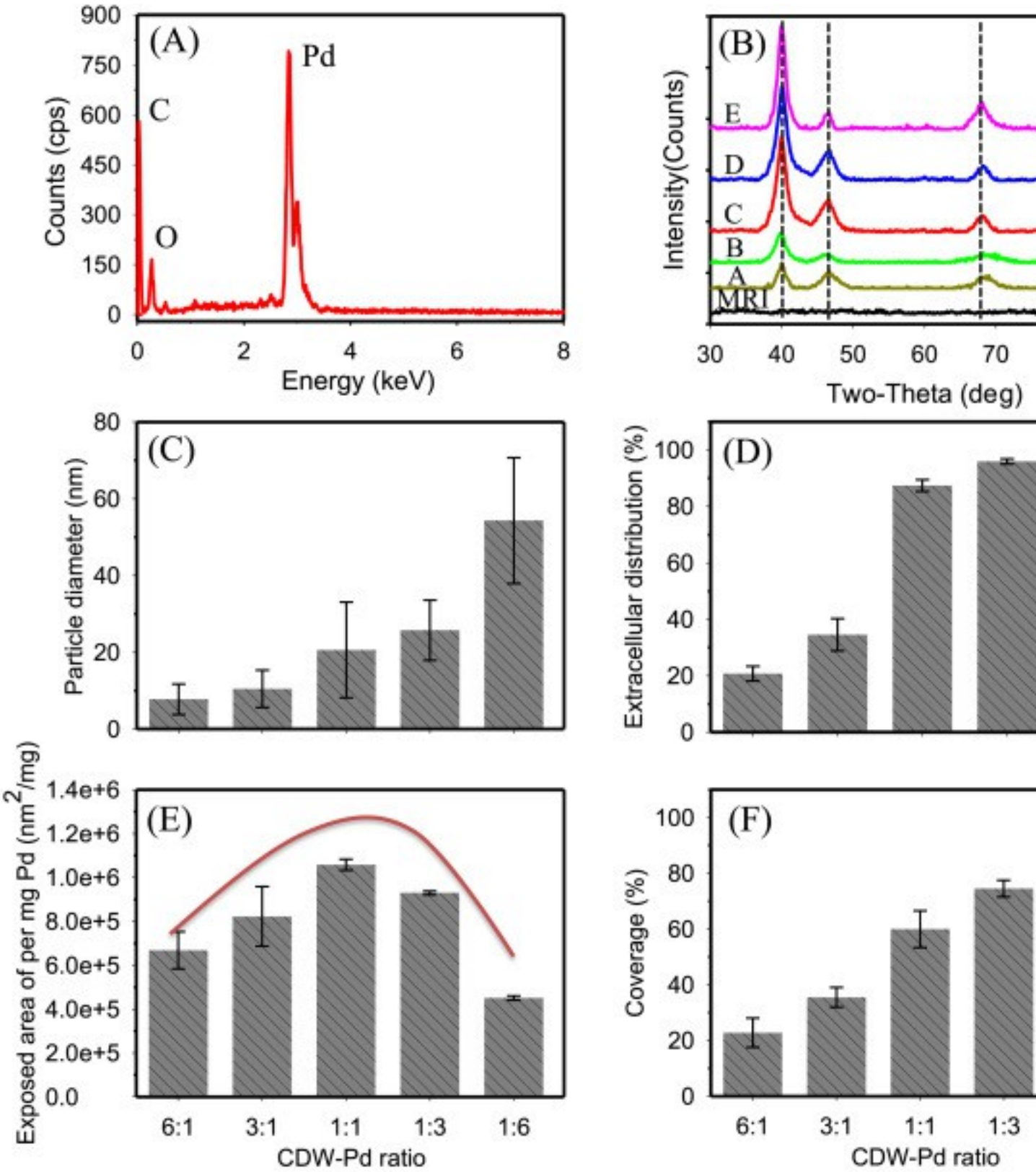

1. Download high-res image (932KB)
2. Download full-size image

Fig. 3. (A) The EDS spectrum of Pd-cell catalyst with CDW:Pd at 1:1 (B) XRD pattern of Pd-cells with different CDW:Pd; (C) The distribution of Pd NPs diameter size, (D) extracellular distribution, (E) exposed area of per milligram Pd and (F) the coverage of Pd NPs on cell surface, all measured by TEM observation of Pd-cell at different CDW:Pd ratios. The red curve in figure E represents the trend line. (For interpretation of the references to colour in this figure legend, the reader is referred to the web version of this article.)

To further evaluate the sizes and distributions of the Pd NPs that were formed, samples after ultrathin section treatment were observed using TEM (Fig. 2, K-O). It could be found that the lower CDW:Pd ratio resulted in the larger NPs size and the higher degree of extracellular distribution (i.e. more NPs distributed at the cellular outer membrane rather than at the periplasmic and cytoplasmic space) (Fig. 3C and D). This was especially obvious for Pd-cells in group E (with CDW:Pd ratios of 1:6) which exhibited the largest average size (54.3 ± 16.4 nm) and highest extracellular distribution degree (~98%). In addition to the fact that the size of NP grew gradually from Fig. 2K to O, it has also been observed that some cells in group E are shown to be distorted and damaged (Fig. 2O), which might be mainly caused by metal toxicity due to excessive deposition of Pd NPs and high concentration of Pd(II) used in synthesis stage.

In Fig. 2O, some Pd NPs with large aggregation can be also observed away from the bacterial cells, which was likely due to the released enzymesform broken cells providing additional nucleation sites for Pd formation outside the cells.

The ratio of CDW:Pd also determined the exposed area of Pd NPs and the coverage of Pd NPs on cell surface as shown in Fig. 3E and F. The exposed area refers to the relatively effective contact area of Pd to the substrate, which play a crucial role in catalysis. According to the estimation method, the exposed area of Pd depends on the NPs size and extracellular distribution. The results indicated that Pd-cell-C (with CDW:Pd ratios of 1:1) held the highest specific exposed area ($10.6 \pm 0.3 \times 10^5$ nm^2 mg^{-1}), which was followed by Pd-cell-D ($9.3 \pm 0.1 \times 10^5$ nm^2 mg^{-1}), while the specific exposed area in Pd-cell-E was the lowest ($4.5 \pm 0.1 \times 10^5$ nm^2 mg^{-1}). The coverage of Pd NPs on cell surface appears as an increase trend with decreasing the CDW:Pd ratio. Pd-cell-E (with CDW:Pd ratios of 1:6) exhibited the greatest coverage (>95%), which enabled a well contact of Pd NPs to each other.

3.2. Catalytic activity of suspended Pd-cell catalysts in solution

The catalytic capabilities of the biosynthesized Pd NPs were tested via the reduction of nitrobenzene (NB) to aniline (AN) in the presence of excessive electron donor, which

were $NaBH_4$in this study. Although $NaBH_4$ is a strong reductant, no obvious decrease of NB concentration was observed without addition of Pd-cell catalyst (blank in Fig. 4). We found that the reaction kinetics can be best fitted using a pseudo-first-order model with respect to the concentration of NB. Typical plots of $-\ln (C_t/C_0)$ against the reaction time for different Pd-cell catalysts were shown in Fig. 4a, where C_t and C_0 are the NB concentrations at time t and 0, respectively. The values of kinetic rate constant k determined from linear regression of $-\ln (C_t/C_0)$ versus reduction time in minutes (Table 2). The catalytic activities of these Pd-cell catalysts for NB reduction were found to follow the order of: D > C > B > A > E. The rate constant of NB reduction for group E (CDW:Pd at 1:6, 0.029 min^{-1}) is very close to that of group A (CDW:Pd at 6:1, 0.031 min^{-1}). Remarkably, the rate constants from group A to group D showed positive dependence on nanoparticle size.

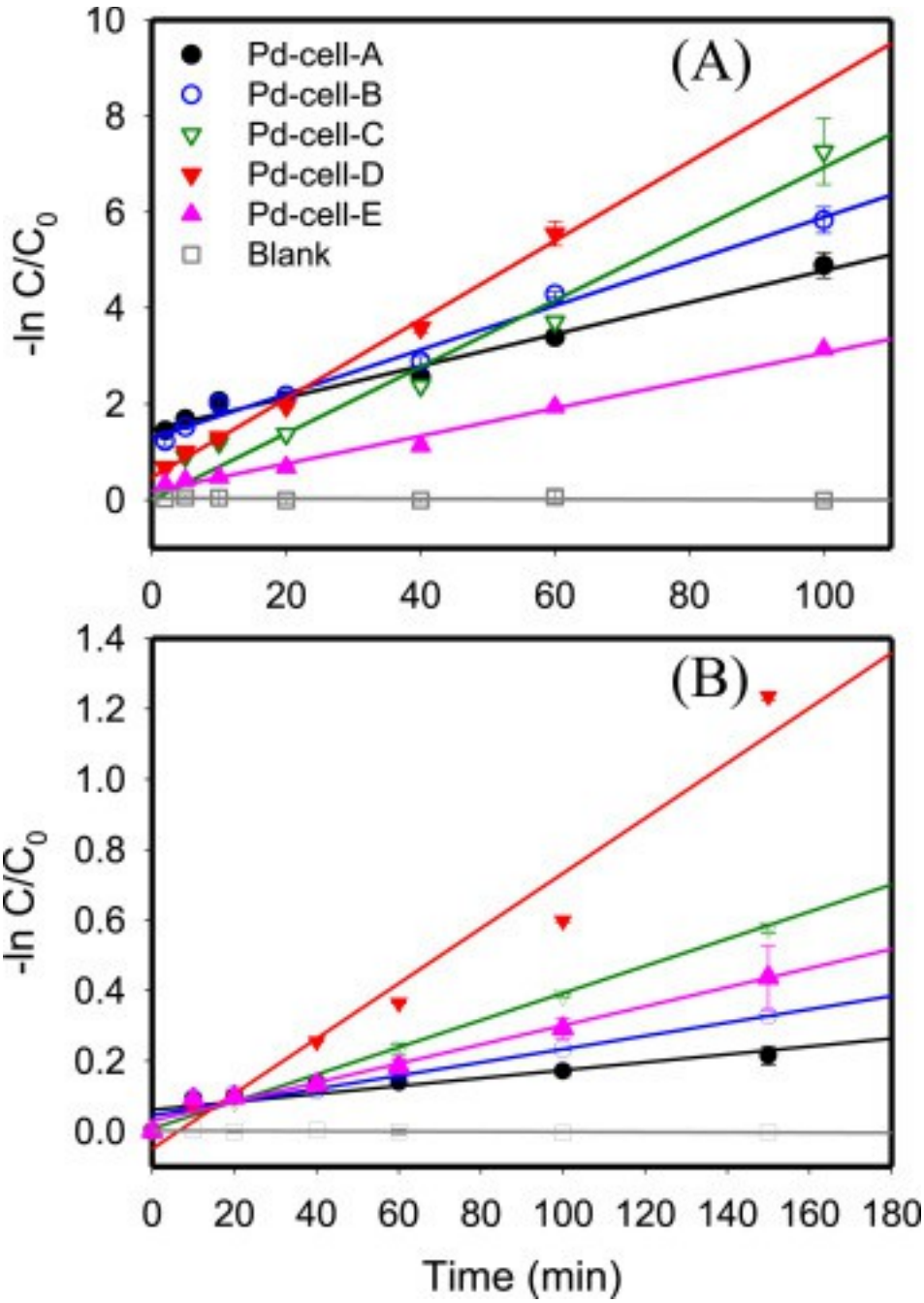

1. Download high-res image (442KB)
2. Download full-size image

Fig. 4. Catalytic performances of Pd-cell used as suspension catalysts. Plots of $\ln(C_t/C_0)$ versus time for the reduction of (A) NB and (B) 4-CP by $NaBH_4$ in the presence of different CDW:Pd ratios. Error bars represented standard deviation (n = 3).

Table 2. Pseudo-first-order rate constant and R^2 for nitrobenzene(NB) and *p*-chlorophenol (4-CP) reduction with different cell dry weight to Pd ratios of Pd-cell used as suspension catalysts and the catalytic current density for electrocatalysis reduction of NB and 4-CP, respectively.

Pd-cell catalyst		Rate constant k (min^{-1})	R2	Catalytic current density ($mA\ cm^{-2}$)
Group A	NB	0.031	0.983	$-6.54 \pm 0.38 \times 10^{-3}$
	4-CP	1.126×10^{-3}	0.896	$-8.91 \pm 1.17 \times 10^{-3}$
Group B	NB	0.046	0.987	$-7.23 \pm 0.46 \times 10^{-3}$
	4-CP	1.885×10^{-3}	0.969	$-10.37 \pm 0.96 \times 10^{-3}$
Group C	NB	0.069	0.999	$-9.69 \pm 0.21 \times 10^{-3}$
	4-CP	3.854×10^{-3}	0.996	$-11.60 \pm 1.46 \times 10^{-3}$
Group D	NB	0.082	0.995	$-10.57 \pm 0.65 \times 10^{-3}$
	4-CP	7.824×10^{-3}	0.966	$-11.63 \pm 1.41 \times 10^{-3}$
Group E	NB	0.029	0.988	$-32.12 \pm 0.64 \times 10^{-3}$
	4-CP	2.708×10^{-3}	0.990	$-33.78 \pm 0.52 \times 10^{-3}$

In addition to the reduction of nitro-group of NB, the Pd-cell catalysts were also tested for their activity towards catalyzing the dechlorination reaction, using the *p*-chlorophenol (4-CP) as typical chloride aromatic pollutants. The catalytic efficiencies of Pd-cell catalysts for 4-CP reduction followed the order of: D > C > E > B > A. The highest reduction k value was also observed in Pd-cell from group D (CDW:Pd at 1:3, 7.8×10^{-3} min^{-1}). For Pd-cell from group E (CDW:Pd at 1:6), the reduction reaction constant (2.7×10^{-3} min^{-1}) was 2.4 and 1.4-fold higher than those Pd-cell from group A and B, respectively, while lower than Pd-cell-D (Fig. 4b). The normalized catalytic rate constant of Pd-cell from group D (CDW:Pd at 1:3) was calculated as 3.9 L $min^{-1} \cdot g^{-1}$, which is higher than the values that previously reported in chemically synthesized Ni@Pd/KCC-1 (1.88 L $min^{-1} \cdot g^{-1}$) and PdAl-IMP-1.5 (2.33 L $min^{-1} \cdot g^{-1}$)(Dong et al., 2015, Molina et al., 2009).

Compared to NB reduction, different substitutes and the position of substitute groups of 4-CP impacted the reduction efficiency of Pd NPs. As a general trend, the reduction efficiencies of nitro- and chloro-aromatic compounds are basically positively correlated to the exposed area, which was controlled by Pd NPs size and the extracellular distribution. However, although Pd-cell-D exhibited the greatest catalytic efficiency, its

exposed area of Pd NPs was not the largest but lower than that in Pd-cell-C. As suggested by Corte et al., the catalytic activity of Pd NPs on cell surfaces could be negatively impacted by a poisoning effect brought from the sulfur compounds contained in cell proteins(De Corte et al., 2013). That means not all of the exposed Pd NPs were capable of being active, especially for those prepared at high CDW:Pd ratios with higher content of biomass. In all, the findings in the scenario of Pd-cell as suspended catalyst suggests it would be controllable to enhance catalytic activity of Pd-cells towards reductive degradation of recalcitrant contaminants by regulating the relationship of NPs size and distribution.

3.3. Electrocatalytic activity of Pd-cell as electrochemical catalyst

The electrocatalytic activity of Pd-cell catalysts were first evaluated in catalyzing hydrogen evolution reaction (HER) by cyclic voltammetry (CV) and chronoamperometry (CA) in N_2saturated phosphate buffer solution (PBS, pH = 7.0) with the identical Pd loading mass on the electrodes. As shown in Fig. 5a, the much higher cathodic catalytic current was observed in the electrode coated with Pd-cells from group E (CDW:Pd-1:6), which was aroused by the adsorbed/absorbed hydrogen and HER(Hou et al., 2016). The adsorbed/absorbed hydrogen was re-oxidized and contributed to the anodic peak at about −0.45 V in anodic sweep. At −1.0 V (in HER range), the catalytic current density of Pd-cell-E catalyst coated electrode is shown as the highest, while the other groups of Pd-cells are much lower with the current density at −1.0 V negatively correlating to the CDW:Pd ratios (D > C > B > A, inset in Fig. 5a and Table 2). As observed in CA tests (at −0.7 V, Fig. 5b), the steady current density of Pd-cell-E coated electrode was 29.5, 11.0, 9.45 and 6.39 times higher than that of group A, B, C and D, respectively, further confirming its high catalytic activity for HER.

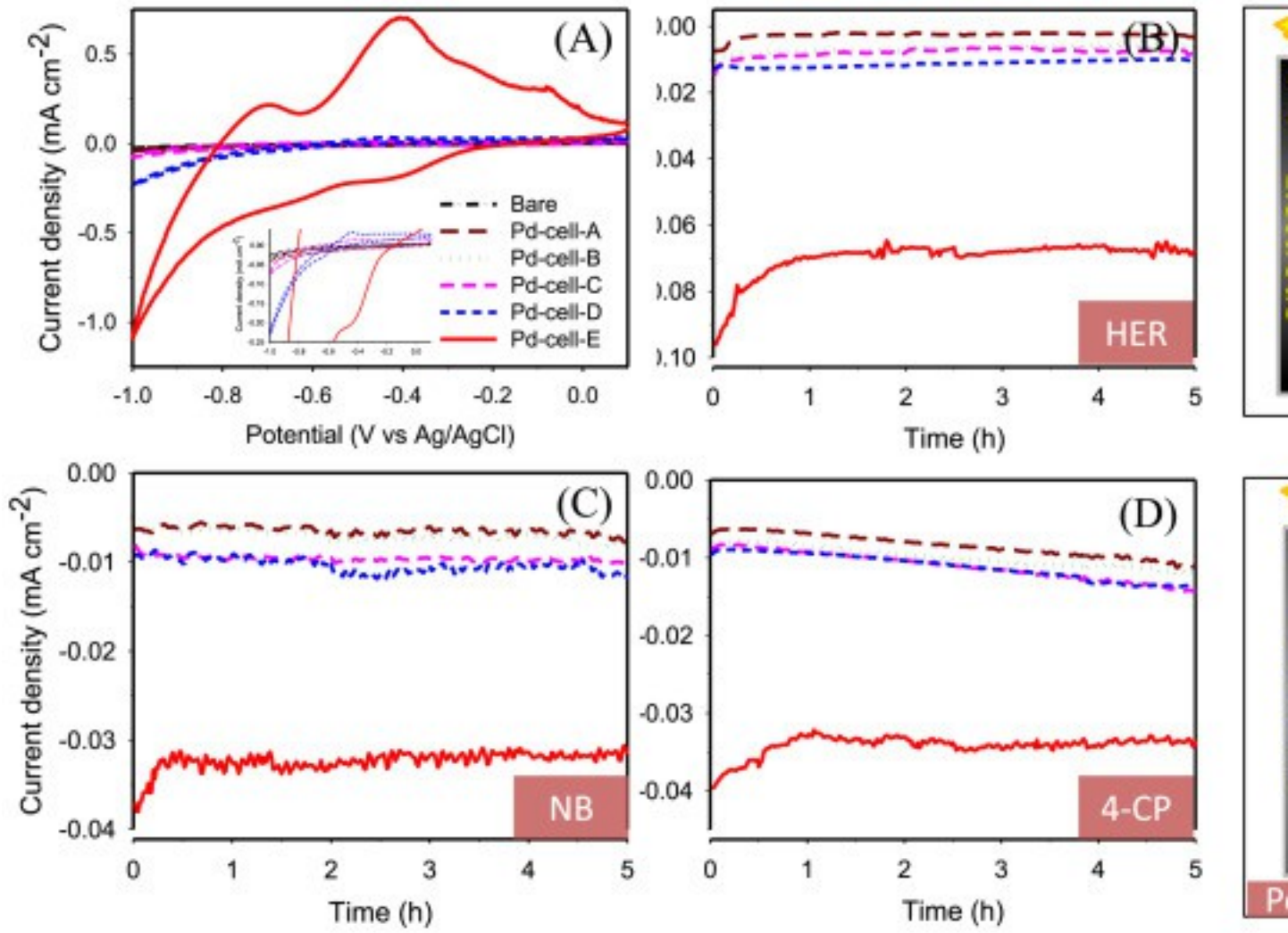

1. Download high-res image (804KB)
2. Download full-size image

Fig. 5. Catalytic performances of Pd-cell used as electrochemical catalysts. (A) Cyclic voltammograms of Pd-cell catalysts at different CDW:Pd ratios coated electrodes in PBS (50 mM). Inset: the corresponding X, Y-axis expansion. The tests were operated under N_2 saturation condition at 30 °C with the scan rate of 10 mV s^{-1}; chronoamperometry analysis of coated electrodes (B) at potential of −0.7 V in PBS (50 mM), (C) at −0.55 V in NB (0.5 mM) amended PBS and (D) at −0.55 V in 4-CP (0.5 mM) amended PBS; schematic illustration of the electron transfer pathway between Pd-cell catalyst and electrode toward HER, NB and 4-CP catalytic reduction for (E) group A, B, C, D and (F) group E coated electrodes, respectively.

To study the electrocatalytic performance of different Pd-cells towards the reductively degrading contaminants (NB and 4-CP), CA tests were performed in N_2-saturated solution of 0.5 mM NB and 0.5 mM 4-CP amended PBS, respectively. The electrode

potential was controlled at −0.55 V (positive to the potential of HER in theory) to ensure the contaminants reduction via a direct electrochemical process rather than mediated by molecule hydrogen (Fig. 5C and D). The results showed that Pd-cell from group E generated the highest current densities for both NB reduction (about 0.032 mA cm^{-2}) and 4-CP reduction (about 0.034 mA cm^{-2}) as compared to other groups of Pd-cells, which exhibited remarkable difference from the catalytic performance order in suspension catalysis system. Because the under potential deposition of hydrogen only occur in Pd NPs that are electrically connected to the electrode (Hou et al., 2016), these results clearly indicated the more efficient electron transfer between Pd NPs and electrode in group E. The main reason could be inferred as its higher electrical conductivity, which is likely contributed by the unique Pd NPs distribution features (i.e. forming a conductive Pd layer on the cell surface) in Pd-cell-E.

In order to shed light on explaining the varied electrocatalytic performance observed in different groups of Pd-cells, the electrochemical active surface areas (ECSA) of these Pd-cell catalysts were further estimated based on the CV curves as shown in Fig. 6a. The reduction peak observed at 0.05 V has been well documented as the reduction of Pd oxide layer (produced during positive scanning) and was employed for the estimation of ECSA according to Eq (2)(Kiyani et al., 2016, Guo et al., 2013). Pd-cell-E (10.6 m^2 g^{-1}) displayed more than 10 times higher ECSA than Pd-cell-D (0.96 m^2 g^{-1}) and Pd-cell-C (0.65 m^2 g^{-1}). The reduction peaks of Pd oxide in Pd-cell-A and Pd-cell-B were negligible, indicating their poor electrochemical activities. The much higher ECSA of Pd-cell-E suggests its superior electrochemical activity, which is consistent with its higher electrocatalytic performance observed in HER as well as in the reduction of NB and 4-CP.

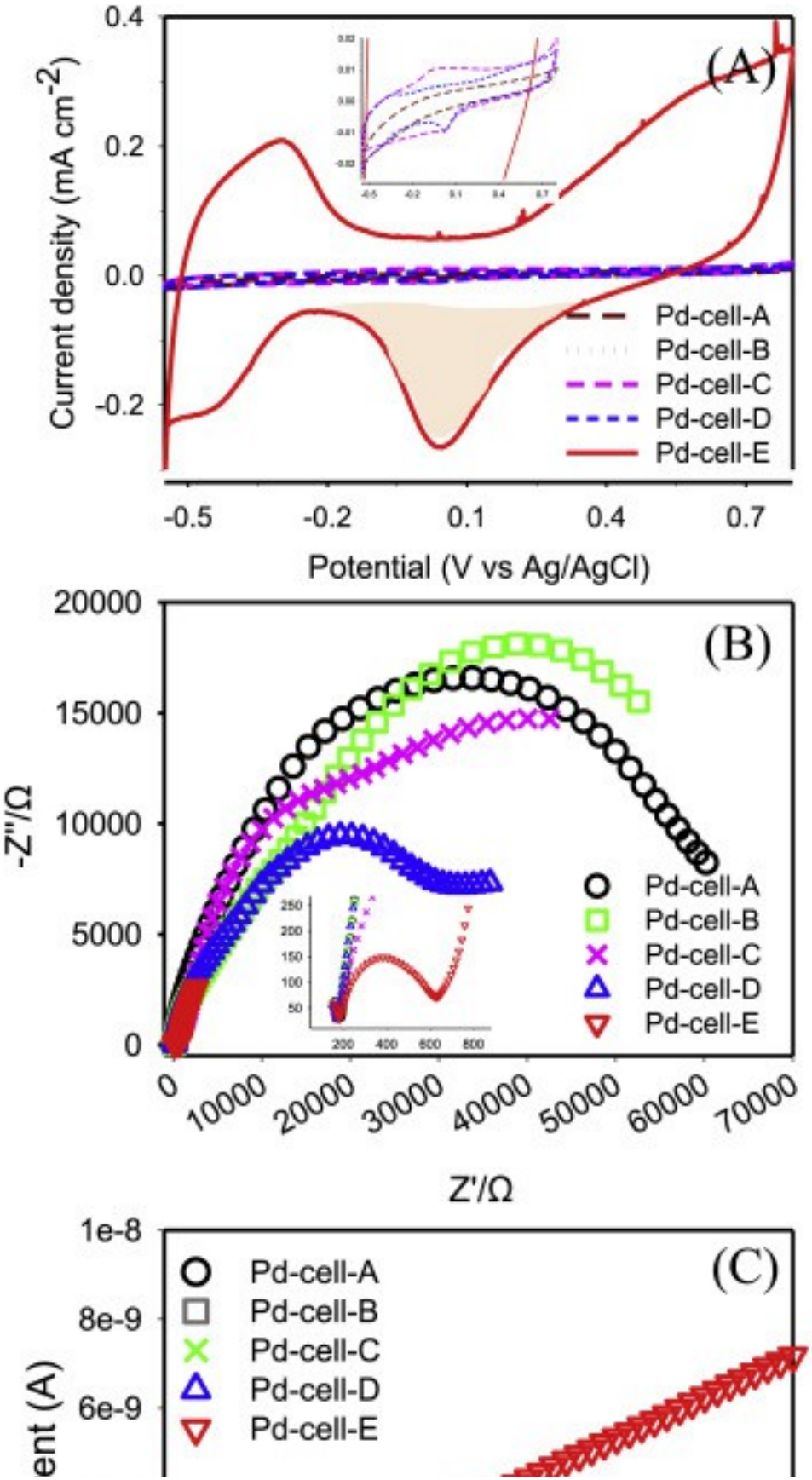
(A)
Current density (mA cm-2)
0.4
0.2
0.0
-0.2
-0.5
-0.2
0.1
0.4
0.7
Potential (V vs Ag/AgCl)
Pd-cell-A
Pd-cell-B
Pd-cell-C
Pd-cell-D
Pd-cell-E
(B)
-Z''/Ω
20000
15000
10000
5000
0
0
10000
20000
30000
40000
50000
60000
70000
Z'/Ω
Pd-cell-A
Pd-cell-B
Pd-cell-C
Pd-cell-D
Pd-cell-E
(C)
1e-8
8e-9
6e-9
Pd-cell-A
Pd-cell-B
Pd-cell-C
Pd-cell-D
Pd-cell-E

1. Download high-res image (887KB)
2. Download full-size image

Fig. 6. (A) Cyclic voltammograms of coated electrodes in N_2-saturated PBS at the scan rate of 10 mV s^{-1}; (B) Nyquist plots of in N_2-saturated solution of 50 mM PBS; (C) I-V curves of coated SPGEs with different CDW:Pd ratios; Insets show the enlarged view.

Furthermore, the interfacial reactions and electrical conductivity performance of synthesized Pd-cell catalysts were investigated using electrochemical impedancespectroscopy (EIS)(An et al., 2013). The impedance spectra (Nyquist plots) of the samples were shown in Fig. 6b. A typical shape with a semicircle was observed in the high frequency region corresponding to charge transfer resistance of electrode(Xu et al., 2014). It was found that the semicircular diameter of the Pd-cell catalyst from group E was considerably much smaller than those of other groups of Pd-cells, suggesting the faster reaction rate and higher efficiency in charge transport(Zhou et al., 2016a). Meanwhile, customized screen-printed gold electrodes (SPGE) were used for measuring the conductivities of the samples. The current profiles as a function of voltage applied across the gap were shown in Fig. 6C. According to Eq (3), the conductivity of Pd-cell from group E (estimated as 0.37 μS cm^{-1}) is dramatically higher than that of other groups of Pd-cells (approaching zero because of the negligible current production with increasing the voltage). This result provided direct evidence that the best electrocatalytic performance of Pd-cell catalyst from group E was mainly due to its good conductivity that facilitated the electron transfer between Pd NPs and electrode.

3.4. Size and distribution effects on suspension and electrocatalytic scenarios

In view of using Pd-cell as suspended catalyst in solution, group D (CDW:Pd at 1:3) exerted the greatest reaction rate towards the catalytic reduction of hydrophobic contaminants NB and 4-CP. As observed in this work, the CDW to Pd ratio strongly affected both of the size and distribution of the formed Pd NPs. The Pd-cell catalyst prepared at 1:3 CDW:Pd ratio was characterized as relative big Pd particle size (25.8 ± 7.8 nm), while its larger extracellular distribution property for Pd NPs (~96%), resulted in the larger exposed area of Pd (9.3 ± 0.1 × 10^5 nm^2 mg^{-1}). High exposed area of Pd NPs was suggested to greatly increase its contact area to hydrophobic molecules(De Windt et al., 2006), which is also expected to provide more sites for the dissociative adsorptionof H_2 (generated from the decomposition of NaBH4) into activating hydrogen (Conrad et al., 1974) and consequently facilitated the reductive of NB and 4-CP. Under the higher ratio of CDW:Pd (group A and B) Pd NPs were formed with much smaller size and mostly embedded into the cells. The limited exposed area,

therefore depressed its catalytic activity. For Pd-cells from group C, the exposed area was estimated to be the largest, while its catalytic performance was lower than that of Pd-cell-D. This indicates there was a deviation between the estimated exposed area and the actual value. In addition, the poisoning effect by sulfur compounds contained in cell proteins and the extracellular polymer encapsulation may also negatively affect the catalytic activity of Pd especially when more biomass was involved. When the CDW:Pd ratio declined from 1:3 to 1:6, a great increase of Pd size and high degree of aggregation of Pd NPs were observed. It had been reported that the initial removal of Pd(II) by biomass was through biosorption and metabolic processes(Windt et al., 2005, Zhou et al., 2016b). After the Pd NPs was synthesized, the formed bioPd will further serve as nucleation sites for the fast growth of Pd NPs through a chemically "auto-catalysis" process(Hou et al., 2016, Baxter-Plant et al., 2003). Under such low CDW:Pd ratio condition (group E at 1:6), the number of nucleation site may be seriously limited due to the much lower content of biomass. As a result, the Pd(II) reduction would be mainly via the growth of Pd and led to the formed Pd NPs have much bigger size. Additionally, less biomass also featured less functional sites for dispersing the reduced Pd(0) nucleus(Zhou et al., 2016b). Thus, the Pd NPs originated from these nuclei would be inclined to form aggregates. The large particle size and the aggregation effect could significantly reduce the specific surface area of Pd NPs, which could explain the decrease of the exposed area and catalytic activity in the Pd-cell from group E. In general, the particle size and distribution of the Pd NPs can be controlled by adjusting the ratio of CDW to Pd, which determines the exposed area of Pd NPs to influence the catalytic activity in the suspension system. By establishing the relationship between exposure area with particle size and distribution, it can provide guidance for the synthesis and application of Pd-cell to maximize the catalytic activity in the suspension scenario.

As described above, the CDW to Pd ratio not only determined the particle size and distribution but also impacted the coverage of deposited Pd NPs on the cell surface. Pd-cells prepared with high CDW:Pd ratios (6:1 and 3:1) were characterized as relative small size Pd NPs (almost less than 10 nm) and low coverage (almost lower than 35%). With regard to the electrocatalytic scenarios, Pd-cells with large fraction of uncovered cell membrane would reduce the chance of interconnection of the cell supported Pd NPs. Particularly, when Pd-cell catalyst was coated on GCE directly, the cell supported Pd NPs would stack on electrode surface layer by layer. The limited electron delivery from electrode to Pd will be caused by the poor conductive nature of *S. oneidensis*cells(Hou et al., 2016, Xiong et al., 2015). (schematic illustration

in Fig. 5 E) The improvement in catalytic current of Pd-cell-E correlated to the largest Pd NPs size distribution (54.3 ± 16.4 nm) and high coverage (>95%) property. When the bacterial cells are wrapped by Pd NPs, the cell supported Pd NPs would be well interconnected. In this way, a conductive path can be established by these Pd NPs and the electrochemical activity of Pd-cells would not be limited by the poor electrical conductivity of the bacterial matrix (schematic illustration in Fig. 5F).
In suspension catalytic system, the catalytic activity was mainly determined by the exposed area of the NPs, while, in the electrocatalytic scenario, the catalytic performance was mainly governed by the coverage of Pd NPs on the cell surface. This indicates that different principles should be applied on the design of bioPd catalysts to enable they are effective for different catalysis systems. As demonstrated in this study, synthesis of Pd-cells by simply adjusting the CDW: Pd ratio is a feasible approach to control the properties of cell supported Pd NPs.

4. Conclusion

In summary, the bioPd NPs with different sizes and distribution properties were synthesized by *S Oneidensis* MR-1 and the catalytic activity of Pd-cells prepared at different CDW:Pd ratios were investigated in two different catalytic systems. The results indicated that (I) the ratio of CDW:Pd determined the average size, extracellular distribution and coverage of Pd NPs on cell surface. Decreasing the CDW:Pd ratio resulted in the increase of NPs size, extracellular distribution degree and the coverage of Pd NPs deposited on cell surface; (II) A specific expression of exposed area-NPs sizes-extracellular distribution relationship was established, which has a direct correlation with the catalytic activity for suspension biocatalysts. The Pd-cell from group D with average diameter at 25.8 ± 7.8 nm and higher exposed area ($9.3 \pm 0.1 \times 10^5$ nm^2 mg^{-1} Pd), exhibited the highest catalytic performance towards reduction of NB and 4-CP aromatic compounds in suspension scenario. When increasing the size of Pd NPs over 50 nm, the reducing of exposed area became a major factor in limiting the catalytic activity; (III) the extracellular distribution and the coverage of Pd NPs on the cell surface played a crucial role in boosting the conductivity of biocatalyst, thus determining the possibility of Pd-cell serving as electrocatalyst. These results shed light on the underlying relationship between the catalytic activity with nano size as well as distribution of Pd NPs on cell surface in different Pd-cell catalytic system. More importantly, this work provided a guideline of designing and developing effective bioPd catalyst in response to different types of catalysis systems. These

principles outlined here are expected to be also helpful for other biogenetic metal systems, enabling the synthesis of bio-NPs effective and suitable for a target system with enhanced catalytic performance.

Acknowledgements

Acknowledgement is made to the financial support of Natural Science Foundation of China (Grant No. 31370157, 21407164and 21577162), National Science Foundation for Distinguished Young Scholars (Grant No. 51225802). HIT Environment and Ecology Innovation Special Funds (No. HSCJ201621).

Appendix A. Supplementary data

The following is the supplementary data related to this article:

Download Word document (3MB)Help with docx files

References

An et al., 2013

H. An, L. Pan, H. Cui, B. Li, D. Zhou, J. Zhai, Q. Li**Synthesis and performance of palladium-based catalysts for methanol and ethanol oxidation in alkaline fuel cells**

Electrochim. Acta, 102 (2013), pp. 79-87

ArticleDownload PDFView Record in Scopus

And and Reinhard, 1999

G.V.L. And, M. Reinhard**Hydrodehalogenation of 1- to 3-carbon halogenated organic compounds in water using a palladium catalyst and hydrogen gas**

Environ. Sci. Technol., 33 (11) (1999), pp. 1905-1910

Baxter-Plant et al., 2003

V.S. Baxter-Plant, I.P. Mikheenko, L.E. Macaskie**Sulphate-reducing bacteria, palladium and the reductive dehalogenation of chlorinated aromatic compounds**

Biodegradation, 14 (2) (2003), pp. 83-90

CrossRefView Record in Scopus

Chaplin et al., 2012

B.P. Chaplin, M. Reinhard, W.F. Schneider, C. Schüth, J.R. Shapley, T.J. Strathmann, C.J. Werth **Critical review of Pd-Based catalytic treatment of priority contaminants in water**

Environ. Sci. Technol., 46 (7) (2012), pp. 3655-3670

CrossRefView Record in Scopus

Conrad et al., 1974

H. Conrad, G. Ertl, E.E. Latta**Adsorption of hydrogen on palladium single crystal surfaces**

Surf. Sci., 41 (2) (1974), pp. 435-446

ArticleDownload PDFView Record in Scopus

Cortese and Heck, 1977

N.A. Cortese, R.F. Heck**Palladium catalyzed reductions of halo-and nitroaromatic compounds with triethylammonium formate**

J. Org. Chem., 42 (22) (1977), pp. 3491-3494

CrossRefView Record in Scopus

Davie et al., 2006

M.G. Davie, M. Reinhard, J.R. Shapley**Metal-catalyzed reduction of N-nitrosodimethylamine with hydrogen in water**

Environ. Sci. Technol., 40 (23) (2006), p. 7329

CrossRefView Record in Scopus

De Corte et al., 2013

S. De Corte, S. Bechstein, A.R. Lokanathan, J. Kjems, N. Boon, R.L. Meyer**Comparison of bacterial cells and amine-functionalized abiotic surfaces as support for Pd nanoparticle synthesis**

Colloids Surf. B. Biointerfaces, 102 (2013), pp. 898-904

ArticleDownload PDFView Record in Scopus

De Gusseme et al., 2011

B. De Gusseme, T. Hennebel, L. Vanhaecke, M.Soetaert, J. Desloover, K. Wille, K. Verbeken, W. Verstraete, N.Boon**Biogenic palladium enhances diatrizoate removal from hospital wastewater in a microbial electrolysis cell**

Environ. Sci. Technol., 45 (13) (2011), pp. 5737-5745

CrossRefView Record in Scopus

De Windt et al., 2006

W. De Windt, N. Boon, J. Van den Bulcke, L.Rubberecht, F. Prata, J. Mast, T. Hennebel, W. Verstraete**Biological control of the size and reactivity of catalytic Pd (0) produced by Shewanella oneidensis**

Ant. Van Leeuwenhoek, 90 (4) (2006), pp. 377-389

CrossRefView Record in Scopus

Deplanche et al., 2014

K. Deplanche, J.A. Bennett, I.P. Mikheenko, J.Omajali, A.S. Wells, R.E. Meadows, J. Wood, L.E. Macaskie**Catalytic activity of biomass-supported Pd nanoparticles: influence of the biological component in catalytic efficacy and potential application in 'green' synthesis of fine chemicals and pharmaceuticals**

Appl. Catal. B Environ., 147 (2014), pp. 651-665

ArticleDownload PDFView Record in Scopus

Deplanche et al., 2010

K. Deplanche, I. Caldelari, I.P. Mikheenko, F.Sargent, L.E. Macaskie**Involvement of hydrogenases in the formation of highly catalytic Pd(0) nanoparticles by bioreduction of Pd(II) using Escherichia coli mutant strains**
Microbiology, 156 (Pt 9) (2010), p. 2630
CrossRefView Record in Scopus

Dong et al., 2015

Z. Dong, X. Le, C. Dong, W. Zhang, X. Li, J. Ma**Ni@ Pd core–shell nanoparticles modified fibrous silica nanospheres as highly efficient and recoverable catalyst for reduction of 4-nitrophenol and hydrodechlorination of 4-chlorophenol**
Appl. Catal. B-Environ, 162 (2015), pp. 372-380
ArticleDownload PDFView Record in Scopus

Guo et al., 2013

S. Guo, S. Li, T. Hu, G. Gou, R. Ren, J. Huang, M. Xie, J.Jin, J. Ma**Graphene decorated with Pd nanoparticles via electrostatic self-assembly: a highly active alcohol oxidation electrocatalyst**
Electrochim. Acta, 109 (2013), pp. 276-282
ArticleDownload PDFView Record in Scopus

Henneb el et al., 2011

T. Hennebel, J. Benner, P. Clauwaert, L. Vanhaecke, P. Aelterman, R. Callebaut, N. Boon, W. Verstraete**Dehalogenation of environmental pollutants in microbial electrolysis cells with biogenic palladium nanoparticles**
Biotechnol. Lett., 33 (1) (2011), pp. 89-95
CrossRefView Record in Scopus

Hennebel et al., 2012

T. Hennebel, S. De Corte, W. Verstraete, N. Boon**Microbial production and environmental applications of Pd nanoparticles for treatment of halogenated compounds**
Curr. Opin. Biotechnol., 23 (4) (2012), pp. 555-561
ArticleDownload PDFView Record in Scopus

Hosseinkhani et 2013

B. Hosseinkhani, T. Hennebel, S. Van Nevel, S.Verschuere, M.M. Yakimov, S. Cappello, M. Blaghen, N. Boon**Biogenic nanopalladium based remediation of chlorinated hydrocarbons in marine environments**
Environ. Sci. Technol., 48 (1) (2013), pp. 550-557

Hosseinkhani et

B. Hosseinkhani, A. Nuzzo, G. Zanaroli, F. Fava, N. Boon, F. Fava**Assessment of catalytic dechlorination activity of suspended and immobilized bio-Pd NPs in different marine conditions**
Appl. Catal. B Environ., 168–169 (168) (2015), pp. 62-67
ArticleDownload PDFView Record in Scopus

Hou et al., 2016

Y.-N. Hou, H. Liu, J.-L. Han, W.-W. Cai, J. Zhou, A.-J.Wang, H.-Y. Cheng**Electroactive biofilm serving as the green synthesizer and stabilizer for in situ fabricating 3D nanopalladium network: an efficient electrocatalyst**
ACS Sustain. Chem. Eng., 4 (10) (2016), pp. 5392-5397
CrossRefView Record in Scopus

Kiyani et al., 201

R. Kiyani, S. Rowshanzamir, M.J. Parnian**Nitrogen doped graphene supported palladium-cobalt as a promising catalyst for methanol oxidation reaction: synthesis, characterization and electrocatalytic performance**
Energy, 113 (2016), pp. 1162-1173
ArticleDownload PDFView Record in Scopus

Li et al., 2002

Y. Li, E. Boone, M.A. El-Sayed**Size effects of PVP-Pd nanoparticles on the catalytic Suzuki reactions in aqueous solution**
Langmuir, 18 (12) (2002), pp. 4921-4925

CrossRefView Record in Scopus

Liu et al., 2016

J. Liu, Y. Zheng, Z. Hong, K. Cai, F. Zhao, H. Han**Microbial synthesis of highly dispersed PdAu alloy for enhanced electrocatalysis**
Sci. Adv., 2 (9) (2016), p. e1600858

Macaskie et al.,

L.E. Macaskie, A.C. Humphries, I.P. Mikheenko, V.S.Baxter-Plant, K. Deplanche, M.D. Redwood, J.A. Bennett, J. Wood**Use of Desulfovibrio and Escherichia coli Pd-nanocatalysts in reduction of Cr(VI) and hydrogenolytic dehalogenation of polychlorinated biphenyls and used transformer oil**
J. Chem. Technol. Biotechnol., 87 (10) (2012), pp. 1430-1435
CrossRefView Record in Scopus

Malvankar et al.,

N.S. Malvankar, M. Vargas, K.P. Nevin, A.E. Franks, C. Leang, B.C. Kim, K. Inoue, T. Mester, S.F. Covalla, J.P. Johnson, V.M. Rotello, M.T. Tuominen, D.R. Lovley**Tunable metallic-like conductivity in microbial nanowire networks**
Nat. Nanotech, 6 (9) (2011), pp. 573-579
CrossRefView Record in Scopus

Martins et al., 20

M. Martins, C. Mourato, S. Sanches, J.P. Noronha, M.B.Crespo, I.A. Pereira**Biogenic platinum and palladium nanoparticles as new catalysts for the removal of pharmaceutical compounds**
Water Res., 108 (2017), pp. 160-168
ArticleDownload PDFView Record in Scopus

Mikheenko et al.

I.P. Mikheenko, M. Rousset, S. Dementin, L.E.Macaskie**Bioaccumulation of palladium by Desulfovibrio fructosivorans wild-type and hydrogenase-deficient strains**
Appl. Environ. Microbiol., 74 (19) (2008), p. 6144
CrossRefView Record in Scopus

Mistry et al., 201

H. Mistry, A.S. Varela, S. Kühl, P. Strasser, B.R. Cuenya**Nanostructured electrocatalysts with tunable activity and selectivity**
Nat. Rev. Mater. (2016), p. 16009
CrossRefView Record in Scopus

Molina et al., 200

C. Molina, L. Calvo, M. Gilarranz, J. Casas, J. Rodriguez**Pd–Al pillared clays as catalysts for the hydrodechlorination of 4-chlorophenol in aqueous phase**
J. Hazard. Mater, 172 (1) (2009), pp. 214-223
ArticleDownload PDFView Record in Scopus

Narayanan and S

K.B. Narayanan, N. Sakthivel**Biological synthesis of metal nanoparticles by microbes**
Adv. Colloid Interface Sci., 156 (1) (2010), pp. 1-13
ArticleDownload PDFView Record in Scopus

Nemamcha et al

A. Nemamcha, J.L. Rehspringer, D. Khatmi**Synthesis of palladium nanoparticles by sonochemical reduction of palladium(II) nitrate in aqueous solution**
J. Phys. Chem., B 110 (1) (2006), pp. 383-387
CrossRefView Record in Scopus

Pat-Espadas et a

A.M. Pat-Espadas, E. Razo-Flores, J.R. Rangel-Mendez, F.J. Cervantes**Direct and quinone-mediated palladium reduction by Geobacter sulfurreducens: mechanisms and modeling**
Environ. Sci. Technol., 48 (5) (2014), pp. 2910-2919
CrossRefView Record in Scopus

Sambrook and R

J. Sambrook, D.W. Russell**Molecular Cloning: a Laboratory Manual 3rd Edition**
Coldspring-Harbour Laboratory Press, UK (2001)

Shao et al., 2011

M. Shao, A. Peles, K. Shoemaker**Electrocatalysis on platinum nanoparticles: particle size effect on oxygen reduction reaction activity**
Nano Lett., 11 (9) (2011), pp. 3714-3719
CrossRefView Record in Scopus

Sun et al., 2012

H. Sun, L. Cao, L. Lu**Bacteria promoted hierarchical carbon materials for high-performance supercapacitor**
Energ. Environ. Sci., 5 (3) (2012), pp. 6206-6213
CrossRefView Record in Scopus

Sun and Zeng, 2

S. Sun, H. Zeng**Size-controlled synthesis of magnetite nanoparticles**
J. Am. Chem. Soc., 124 (28) (2002), pp. 8204-8205
CrossRefView Record in Scopus

Tuo et al., 2015

Y. Tuo, G. Liu, B. Dong, J. Zhou, A. Wang, J. Wang, R. Jin, H. Lv, Z. Dou, W. Huang**Microbial synthesis of Pd/Fe3O4, Au/Fe3O4 and PdAu/Fe3O4 nanocomposites for catalytic reduction of nitroaromatic compounds**
Sci. Rep., 5 (2015)

Tuo et al., 2013

Y. Tuo, G. Liu, J. Zhou, A. Wang, J. Wang, R. Jin, H. Lv**Microbial formation of palladium nanoparticles by Geobacter sulfurreducens for chromate reduction**

Bioresour. Technol., 133 (2) (2013), pp. 606-611
ArticleDownload PDFView Record in Scopus

Windt et al., 200

W.D. Windt, P. Aelterman, W. Verstraete**Bioreductive deposition of palladium (0) nanoparticles on Shewanella oneidensis with catalytic activity towards reductive dechlorination of polychlorinated biphenyls**
Environ. Microbiol., 7 (3) (2005), pp. 314-325
CrossRef

Wu et al., 2011

X. Wu, F. Zhao, N. Rahunen, J.R. Varcoe, C. Avignone-Rossa, A.E. Thumser, R.C. Slade**A role for microbial palladium nanoparticles in extracellular electron transfer**
Angew. Chem. Int. Ed. Engl., 50 (2) (2011), pp. 427-430
CrossRefView Record in Scopus

Xiong et al., 201

L. Xiong, J.-J. Chen, Y.-X. Huang, W.-W. Li, J.-F. Xie, H.-Q. Yu**An oxygen reduction catalyst derived from a robust Pd-reducing bacterium**
Nano Energy, 12 (2015), pp. 33-42
ArticleDownload PDFView Record in Scopus

Xu et al., 2014

X. Xu, Y. Zhou, J. Lu, X. Tian, H. Zhu, J. Liu**Single-step synthesis of PtRu/N-doped graphene for methanol electrocatalytic oxidation**
Electrochim. Acta, 120 (2014), pp. 439-451
ArticleDownload PDFView Record in Scopus

Yates et al., 201

M.D. Yates, R.D. Cusick, I. Ivanov, B.E. Logan**Exoelectrogenic biofilm as a template for sustainable formation of a catalytic mesoporous structure**
Biotechnol. Bioeng., 111 (11) (2014), pp. 2349-2354
CrossRefView Record in Scopus

Yong et al., 2002

P. Yong, N.A. Rowson, J.P.G. Farr, I.R. Harris, L.E.Macaskie**Bioreduction and biocrystallization of palladium by Desulfovibrio desulfuricans NCIMB 8307**
Biotechnol. Bioeng., 80 (4) (2002), pp. 369-379
CrossRefView Record in Scopus

Yong et al., 2002

P. Yong, N.A. Rowson, J.P.G. Farr, I.R. Harris, L.E.Macaskie**Bioaccumulation of palladium by Desulfovibrio desulfuricans**
J. Chem. Technol. Biotechnol., 77 (5) (2002), pp. 593-601
CrossRefView Record in Scopus

Zhao et al., 2011

Y. Zhao, L. Zhan, J. Tian, S. Nie, Z. Ning**Enhanced electrocatalytic oxidation of methanol on Pd/polypyrrole–graphene in alkaline medium**
Electrochim. Acta, 56 (5) (2011), pp. 1967-1972
ArticleDownload PDFView Record in Scopus

Zhou et al., 2016

X. Zhou, Y. Liu, H. Ju, B. Pan, J. Zhu, T. Ding, C. Wang, Q. Yang**Design and epitaxial growth of MoSe2–NiSe vertical heteronanostructures with electronic modulation for enhanced hydrogen evolution reaction**
Chem. Mater, 28 (6) (2016), pp. 1838-1846
CrossRefView Record in Scopus

Zhou et al., 2016b

C. Zhou, Z. Wang, A.K. Marcus, B.E. Rittmann**Biofilm-enhanced continuous synthesis and stabilization of palladium nanoparticles (PdNPs)**
Environ. Sci. Nano, 3 (6) (2016), pp. 1396-1404
CrossRefView Record in Scopus

Zhou et al., 2006

W.P. Zhou, A. Lewera, R. Larsen, R.I. Masel, P.S. Bagus, A. Wieckowski**Size effects in electronic and catalytic properties of unsupported palladium nanoparticles in electrooxidation of formic acid**
J. Phys. Chem., B 110 (27) (2006), pp. 13393-13398
CrossRefView Record in Scopus